Molecular Biology of the Cell
Vol. 17, 1364–1374, March 2006

Protein Kinase Cγ Regulates Myosin IIB Phosphorylation, Cellular Localization, and Filament Assembly

Michael Rosenberg and Shoshana Ravid

Department of Biochemistry, Institute of Medical Sciences, Faculty of Medicine, The Hebrew University, Jerusalem 91120, Israel

Submitted July 5, 2005; Revised December 5, 2005; Accepted December 27, 2005
Monitoring Editor: Anne Ridley

Nonmuscle myosin II is an important component of the cytoskeleton, playing a major role in cell motility and chemotaxis. We have previously demonstrated that, on stimulation with epidermal growth factor (EGF), nonmuscle myosin heavy chain II-B (NMHC-IIB) undergoes a transient phosphorylation correlating with its cellular localization. We also showed that members of the PKC family are involved in this phosphorylation. Here we demonstrate that of the two conventional PKC isoforms expressed by prostate cancer cells, PKCβII and PKCγ, PKCγ directly phosphorylates NMHC-IIB. Overexpression of wild-type and kinase dead dominant negative PKCγ result in both altered NMHC-IIB phosphorylation and subcellular localization. We have also mapped the phosphorylation sites of PKCγ on NMHC-IIB. Conversion of the PKCγ phosphorylation sites to alanine residues, reduces the EGF-dependent NMHC-IIB phosphorylation. Aspartate substitution of these sites reduces NMHC-IIB localization into cytoskeleton. These results indicate that PKCγ regulates NMHC-IIB phosphorylation and cellular localization in response to EGF stimulation.

INTRODUCTION

Directed cell migration is a complex process; it requires numerous factors to coordinate the functioning of the cell cytoskeleton so that the cell achieves the necessary polarization for chemotaxis (Lauffenburger and Horwitz, 1996; Mitchison and Cramer, 1996). One of the cytoskeletal proteins that plays an important role in chemotaxis is nonmuscle myosin II (Spudich, 1989; Chung *et al.*, 2001; Postma *et al.*, 2004). In vertebrates, there are at least three nonmuscle myosin II heavy chain (NMHC) genes that encode separate isoforms of the heavy chain: NMHC-IIA, NMHC-IIB, and NMHC-IIC (Katsuragawa *et al.*, 1989; Kawamoto and Adelstein, 1991; Golomb *et al.*, 2004). These myosin II isoforms differ in their heavy chain sequences (Takahashi *et al.*, 1992; Golomb *et al.*, 2004), in the kinetics of ATPase activity (Kelley *et al.*, 1996; Kovacs *et al.*, 2003; Rosenfeld *et al.*, 2003; Wang *et al.*, 2003; De La Cruz and Ostap, 2004; Kim *et al.*, 2005) and in their subcellular localization in various cells types (Maupin *et al.*, 1994; Kelley *et al.*, 1996; Kolega, 1998, 2003; Bao *et al.*, 2005; Kim *et al.*, 2005). Myosin II is a hexamer composed of two heavy chains of ~200 kDa and two pairs of 17- and 20-kDa light chains, and it is regulated by light chain and heavy chain phosphorylation (Tan *et al.*, 1992; Bresnick, 1999; de la Roche and Cote, 2001). Phosphorylation of the regulatory light chains regulates the actin-activated ATPase activity and filament assembly (Bresnick, 1999). Phosphorylation of myosin II heavy chains in the slime mold *Dictyostelium discoideum* inhibits filament assembly (Kuczmarski and Spudich, 1980; Pasternak *et al.*, 1989; Liang *et al.*, 1999). In addition, a number of myosin II heavy chain kinases (NMHCKs), purified from *Dictyostelium* cells, regulate the assembly properties of myosin II heavy chains in vivo (de la Roche and Cote, 2001). However, the mechanisms controlling myosin II heavy chain phosphorylation in mammalian cells are still largely unknown.

In vitro and in vivo studies have shown that heavy chains of NMHC-IIA and NMHC-IIB are phosphorylated by a number of kinases, including protein kinase C (PKC) and casein kinase II (CKII; Kawamoto *et al.*, 1989; Ludowyke *et al.*, 1989; Murakami *et al.*, 1990; Conti *et al.*, 1991; Kelley *et al.*, 1991; Moussavi *et al.*, 1993; Murakami *et al.*, 1995, 1998; Straussman *et al.*, 2001). However, there is still a controversy about the effect of heavy chain phosphorylation on filament assembly of NMHC-IIA and NMHC-IIB. Murakami *et al.* reported that heavy chain phosphorylation by PKC and CKII inhibits filament assembly of NMHC-IIB but not of NMHC-IIA. In contrast, filament assembly of NMHC-IIA is regulated by noncovalent association of Mts1 protein (Murakami *et al.*, 1995, 1998, 2000). Recently, however, filament assembly of NMHC-IIA was shown to be regulated by both heavy chain phosphorylation and by Mts1 (Li *et al.*, 2003; Dulyaninova *et al.*, 2005). Thus, the regulation of NMHC-II by heavy chain phosphorylation remains unclear.

We have shown previously that EGF stimulation of prostate metastatic cells (TSU-pr1 cells) transiently increases phosphorylation of both NMHC-IIA and NMHC-IIB. However, only NMHC-IIB phosphorylation correlated with the EGF-dependent dynamics of the distribution of NMHC-IIB between the cytoplasm and the cell cortex (Straussman *et al.*, 2001). This phosphorylation is carried out by member(s) of the PKC family (Straussman *et al.*, 2001). In addition, overexpression of a short fragment derived from the carboxy terminus of NMHC-IIB, which can undergo phosphorylation but is unable to form filaments, abolished the EGF-dependent NMHC-IIB phosphorylation, thus significantly increasing the amount of NMHC-IIB in the cell cortex (Ben-Ya'acov and Ravid, 2003). These findings were explained by the NMHC-IIB fragment competing with the endogenous

This article was published online ahead of print in *MBC in Press* (http://www.molbiolcell.org/cgi/doi/10.1091/mbc.E05–07–0597) on January 4, 2006.

Address correspondence to: Shoshana Ravid (ravid@cc.huji.ac.il).

NMHC-IIB for the heavy chain kinase(s), resulting in impaired heavy chain phosphorylation and localization.

The experiments presented here provide evidence that protein kinase C γ (PKCγ) directly phosphorylates NMHC-IIB in vitro. Furthermore, overexpression of PKCγ wild type or dominant-negative kinase-dead PKCγ affects NMHC-IIB phosphorylation and cellular localization. Finally, NMHC-IIB with all PKCγ sites replaced by alanine residues shows reduced phosphorylation in vivo. Furthermore replacing these sites with aspartate residues resulted in reduced localization of this mutated NMHC-IIB with the cell cytoskeleton both in TSU-Pr1 cells and in fibroblasts lacking NMHC II-B (Tullio *et al.*, 1997). To our knowledge, this is the first demonstration that an NMHC-IIB kinase in mammalian cells regulates NMHC-IIB function in vivo.

MATERIALS AND METHODS

Cell Lines and Culture Conditions

TSU-pr1 prostate carcinoma cell line (Iizumi *et al.*, 1987) was kindly provided by Dr. A. Passaniti (University of Maryland, National Institutes of Health, Baltimore, MD). TSU-pr1 cells were maintained in RPMI-1640 (Sigma, St. Louis, MO), supplemented with 10% fetal calf serum (FCS) and antibiotics (100 U/ml penicillin, 100 μg/ml streptomycin, and 1:100 Biomyc3 anti-mycoplasma antibiotic solution, all from Biological Industries, Beit HaEmek, Israel).

COS-7 cell line was a kind gift of Dr. R. Hertz (Department of Human Nutrition and Metabolism, Hebrew University Medical School). Fibroblast line lacking NMHC II-B (B^-/B^- MEFs) was a generous gift of Dr. R. S. Adelstein (Laboratory of Molecular Cardiology and Laboratory of Molecular Physiology, National Institutes of Health, Bethesda, MD). Both cell lines were maintained in high-glucose DMEM supplemented with 2 mM L-glutamine, 10% FCS, and antibiotics (100 U/ml penicillin, 100 μg/ml streptomycin, and 1:100 Biomyc3 anti-mycoplasma antibiotic solution (all from Biological Industries).

All cell lines were grown in a humidified atmosphere of 5% CO_2 and 95% air, at 37°C.

Kinase Activity Assay for Recombinant PKC Isoforms

Purified recombinant human PKCβII and PKCγ (Sigma) were dissolved to 20 ng/μl in dilution buffer (10 mM HEPES, pH 7.4, 5 mM DTT, 0.01% Triton X-100). All reactions were performed in 50 μl volume. Substrate mix (10 μl; 20 mM Tris, pH 7.5, 600 mM NaCl, 5 mM EDTA, 1 mM DTT, and 5 μg 70-kDa NMHC-IIB fragment [MHCBrod]; Ben-Ya'acov and Ravid, 2003) were dissolved in 28 μl 10 mM HEPES, pH 7.4. To each reaction mixture 5 μl of activator mix (0.2 mg/ml 1,2-dioleoyl-sn-glycerol [Sigma], 1 mg/ml L-α-phosphatidyl-L-serine [Sigma] and 2 mM $CaCl_2$ in 10 mM HEPES, pH 7.4) and 2 μl (40 ng) of appropriate enzyme was added. The reaction was initiated by the addition of 5 μl of ATP mix (10 mM HEPES, pH 7.4, 1 mM ATP [Roche, Basel, Switzerland], 2.5 μCi of [γ-^{32}P]ATP [Amersham Pharmacia Biotech, Piscataway, NJ] and 100 mM $MgCl_2$). After 7 min of incubation at 30°C the reactions were stopped by the addition of 100 μl ice-cold 40% trichloroacetic acid (TCA). After incubating for 10 min on ice, the precipitated proteins were pelleted for 10 min by centrifugation at 16,000 × *g*. The pellets were washed once with 500 μl ice-cold 5% TCA and 30 μl 2× SDS-PAGE sample buffer (100 mM Tris, pH 6.8, 200 mM DTT, 4% SDS, 0.2% bromophenol blue, 20% glycerol) was added to the reactions and boiled for 5 min at 100°C. The samples were separated on 10% SDS-PAGE and the MHCBrod fragments were visualized by staining with Coomassie-Blue reagent. To determine the amount of phosphate incorporation, the bands of MHCBrod substrate were excised from the gel, transferred to tubes containing 3 ml scintillation liquid, and counted using a scintillation counter. The specific activity for each sample was expressed as the amount of phosphate incorporated into a mole of substrate per min per microgram enzyme.

Autophosphorylation of PKCγ was carried out as described above for kinase assay except that MHCBrod was not added. Kinase assays with myelin basic protein (MBP; Sigma) were performed as described above with minor modifications. Reaction volume was 100 μl and contained 10 μg of MBP dissolved in 78 μl 20 mM HEPES, pH 7.4, and 10 μl of activators mix and 2 μl (40 ng) of appropriate enzyme were added. Reaction was initiated by the addition of 10 μl of ATP mix. After incubation at 30°C for 7 min, the reactions were stopped by the addition of 150 μl ice-cold 40% TCA. After incubating for 10 min on ice, the precipitated proteins were pelleted for 10 min by centrifugation at 16,000 × g. The pellets were washed once with 500 μl ice-cold 5% TCA and 30 μl 2× SDS-PAGE sample buffer was added to the pellets and boiled for 5 min at 100°C. The samples were separated on 12% SDS-PAGE, the MBP were visualized by staining with Coomassie-Blue reagent. The MBP bands excised from the gel and counted using a scintillation counter. The specific activity for each sample was expressed as the amount of phosphate incorporated into a mole of MBP per minute per microgram enzyme.

```
1922
   STLKNRLRRGGPISFSSSRSGRRQLHLEGASLELSDDDTESKTSDVNETQPPQSE - WT

1922
   STLKNRLRRGGPIAFAAARAGRRQLHLEGAALELSDDDTESKTSDVNETQPPQSE - S6A

1922
   STLKNRLRRGGPIDFDDDRDGRRQLHLEGADLELSDDDTESKTSDVNETQPPQSE - S6D
```

Figure 1. The C-terminal sequences of NMHC-IIB proteins that were used in the present study. WT, NMHC-IIB wild type containing the intact protein kinase C γ (PKCγ) phosphorylation sites (S in bold); S6A, NMHC-IIB in which the PKCγ phosphorylation sites were converted to alanine residues (A); S6D, NMHC-IIB in which PKCγ phosphorylation sites were converted to aspartate residues (D).

Construction of PKCγ Wild-Type and Kinase-Dead Fused to Green Fluorescence Protein

The coding sequence of rat brain PKCγ in pBK-CMV phagemid vector (Stratagene, La Jolla, CA) was kindly provided by Dr. A. L. Carvalho (Center for Neuroscience and Cell Biology, University of Coimbra, Portugal). According to NCBI Blast sequence alignment, rat PKCγ has 99% similarity to its human counterpart at the protein level. Rat brain PKCγ coding sequence was excised from pBK-CMV phagemid vector with NheI and XbaI (Fermentas, Vilnius, Lithuania) and inserted into XhoI site of pEGFP-C2 vector (Clontech, San Jose, CA) by blunt end ligation. The dominant-negative kinase-dead PKCγ was created by substitution of the conserved lysine at position 380 in the ATP-binding site with alanine residue using QuikChange Site-directed mutagenesis kit (Stratagene) according to the manufacturer's instructions. The complementary primers (Integrated DNA Technologies, Coralville, IA) used were as follows: sense primer: 5′-GAA CTC TAT GCC ATC GCG ATA CTG AAA AAA GAC GTC ATT GTC C-3′; antisense primer -5′-GGA CAA TGA CGT CTT TTT TCA GTA TCG CGA TGG CAT AGA GTT C-3′. Mutated nucleotides are underlined. The mutations were verified by DNA sequencing (Center for Genomic Analysis, The Hebrew University, Jerusalem).

Construction of NMHC-IIB Mutants

MHCBrod (Ben-Ya'acov and Ravid, 2003) in pET21C vector (Novagen, San Diego, CA) was subjected to series of mutagenesis reactions using the QuikChange Site-directed mutagenesis kit (Stratagene) according to the manufacturer's instructions. The mutations were confirmed by DNA sequencing (Center for Genomic Analysis, The Hebrew University, Jerusalem). To create full-length NMHC-IIB fused to green fluorescent protein (GFP) and carrying the same mutations, mutated MHCBrod in pET21C vector was digested with SmaI (Fermentas), the resulting 1.5-kb fragment of MHBrod was cloned into SmaI-digested plasmid vector pEGFP-C3 (Clontech) containing the entire coding sequence of NMHC-IIB (kindly provided by Dr. R. S. Adelstein, Laboratory of Molecular Cardiology, NIH). The mutants NMHC-IIB used in this study are listed in Figure 1.

Transfections

For transient transfection, cells were plated on 30- or 60-mm tissue culture plates 16 h before the transfection. Transfection was performed with 1 or 4 μg of the plasmid DNA per 30- or 60-mm dish, respectively, using JetPEI Transfection Reagent (Polyplus-transfection, Strasbourg, France) with N/P ratio = 7, according to the manufacturer's instructions. For stable transfection, 4×10^5 TSU-pr1 cells were plated on 30-mm tissue culture dishes ~16 h before the transfection. Cells were transfected with 1 μg of the plasmid DNA according to the same protocol. Stable clones were selected and isolated using 400 μg/ml G418 antibiotics (Calbiochem, San Diego, CA).

Gel Electrophoresis and Western Blot Analysis of GFP-Protein Kinase Cγ Expression

To prepare whole cell extracts, TSU-pr1 cells stably expressing GFP-PKCγ^{WT} or GFP-PKCγ^{DN} were plated on 30-mm tissue culture dishes and grown to 80% confluence at 37°C in a humidified atmosphere. Cells were then washed once with phosphate-buffered saline (PBS), and 100 μl 2× SDS-PAGE sample buffer was added and the lysed cells were scraped, from the dishes, transferred to Eppendorf tubes, and boiled for 5 min at 100°C. Whole cell extracts, 30 μl, were separated on SDS-PAGE using Laemmli's system (Laemmli, 1970). Western blot analysis was performed as described (Straussman *et al.*, 2001). Briefly, the nitrocellulose membrane was blocked with 5% milk-Tris-buffered saline-T and probed with anti-PKCγ mouse monoclonal antibody (mAb; Transduction Laboratories, Lexington, KY). Blots were washed with Tris-buffered saline-T (25 mM Trizma base, 140 mM NaCl, and 0.1% Tween-20) and developed using horseradish peroxidase coupled to a secondary antibody (1:3000; Jackson ImmunoResearch, West Grove, PA). Cells stably ex-

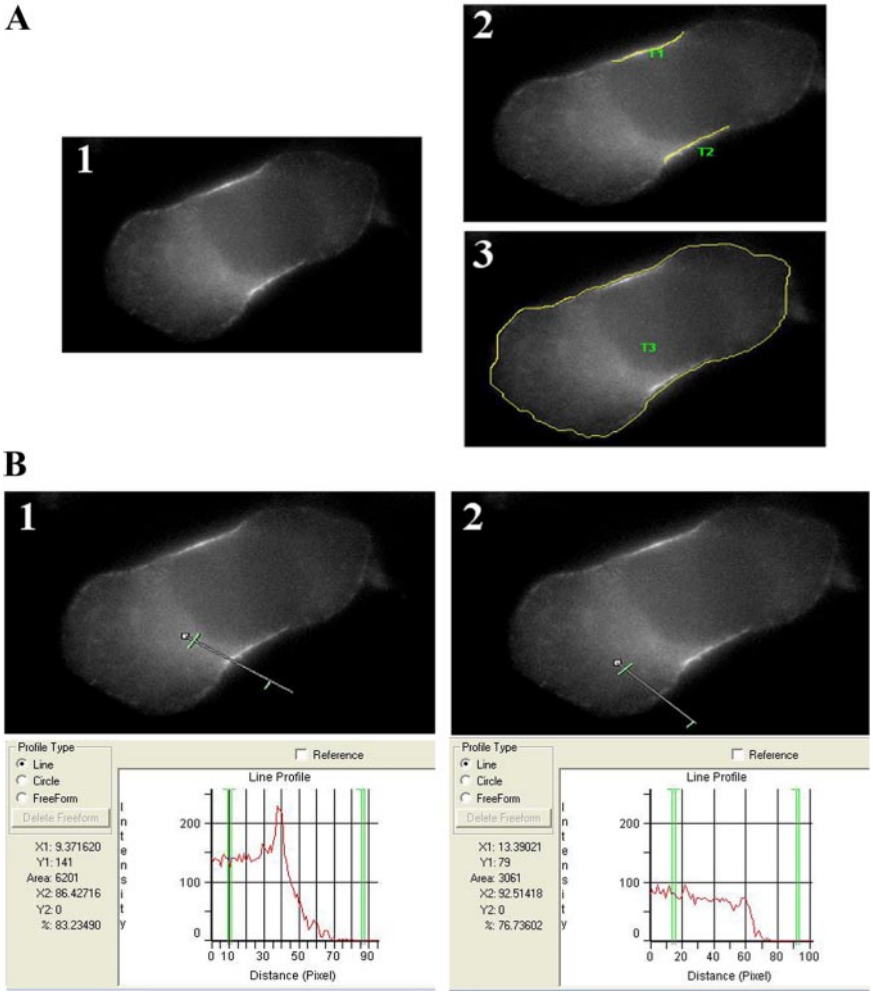

Figure 2. Cortical index measurement. Cells expressing NMHC-IIB tagged with GFP were visualized using fluorescence microscope; images were collected and analyzed using ImagePro software. (A) A representative cell that was used for cortical index measurement (panel 1). The cortical index parameter was determined by measuring the length of cortical area occupied by expressed NMHC-IIB (T1 and T2 in panel 2) and length of entire cortical area (T3 in panel 3), as described in *Materials and Methods*. (B) Line profile function was used to find the areas enriched with expressed NMHC-IIB fused to GFP as described in *Materials and Methods*. Two representative profiles in areas with true enrichment (1) and false enrichment (2) are shown.

pressing GFP only were used as a control. The amount of expressed and endogenous PKCγ was determined by measuring the intensity of the Western blot bands obtained for each protein using FluorS scanning laser densitometer (Bio-Rad, Richmond, CA) and FluorS software. The expression level of recombinant PKCγ was estimated as the ratio of intensities for expressed protein to endogenous protein.

Microscopy

Indirect immunofluorescent staining was carried out as previously described (Ben-Ya'acov and Ravid, 2003). TSU-pr1 cells were grown to 60% confluence on coverslips and double-stained with polyclonal antibody specific for the N-terminal domain of NMHC-IIB (kindly provided by Dr. R. S. Adelstein) and secondary antibody, goat anti-rabbit IgG conjugated to Cy5 (Jackson ImmunoResearch); and anti-PKC-MC5 mouse mAb (Sigma) specific for the hinge domain of conventional PKC isoforms, and secondary antibody goat anti-mouse IgG conjugated to FITC (Jackson ImmunoResearch). TSU-pr1 cells expressing GFP, $PKC\gamma^{WT}$, and $PKC\gamma^{DN}$ were stained with antibody specific for the N-terminal domain of NMHC-IIB only or in combination with rhodamine-phalloidin (Molecular Probes, Eugene, OR). The cells were visualized using a 40× objective under a Zeiss LSM 410 inverted confocal laser scanning system (Thornwood, NY). Confocal images were converted to TIFF format and transferred to a Zeiss imaging workstation for pseudocolor presentation.

For direct fluorescence visualization TSU-pr1 cells transiently transfected with GFP-NMHC-IIB constructs were stimulated for 2 min with 7 ng/ml EGF and fixed for 10 min in 1.5 ml of 3.7% formaldehyde in PBS. After washing three times with 2 ml PBS, cells were mounted on slides using Vectashield mounting medium (Vector Laboratories, Burlingame, CA). The cells were visualized using a 100× objective under an inverted Zeiss Axiovert 200 fluorescence microscope. Images were collected with SensiCam cooled-charged device camera (PCO Computer Optics, Kelheim, Germany), and images were analyzed using ImagePro 4.5.1 software (MediaCybernetics, Silver Spring, MD).

For cortical index measurement, the "Measurements" option in ImagePro 4.5.1 was used as demonstrated in Figure 2A. Length (in units of pixels) of cortical area occupied by expressed NMHC-IIB (T1 and T2) and length of entire cortical area (perimeter of entire cell = T3) were measured. The cortical index was calculated as follows: cortical index = total length of cortical area occupied by expressed NMHC-IIB/perimeter of entire cell. After the labeling in Figure 2A, cortical index of the cell = (T1 + T2)/T3. In the cases where localization of expressed NMHC-IIB into cell cortex was not clear, the "Line profile" function was used as demonstrated in Figure 2B. This function gives the distribution of intensities along the line drawn on the picture. In the areas enriched with cortical NMHC-IIB, there was a significant increase in intensity in the vicinity of cell cortex (Figure 2B, panel 1) compared with areas with false enrichment (Figure 2B, panel 2).

Direct fluorescence visualization of NMHC-IIB tagged with GFP expressed in mouse embryonic fibroblasts (MEFs) deleted for NMHC-IIB was done as follow. 2×10^5 cells were plated on 30-mm tissue culture dishes. Six hours after transfection with GFP-NMHC-IIB construct, 0.75×10^5 cells were replated on coverslips coated with collagen I and incubated for 16 h at 37°C in humidified atmosphere. After washing twice with 1 ml PBS, cells were serum-starved for 24 h in high-glucose DMEM supplemented with 2 mM L-glutamine, 100 U/ml penicillin, 100 μg/ml streptomycin, and 0.1% fatty-acid free bovine serum albumin (Sigma). After starvation, cells were fixed for 10 min in 1.5 ml of 3.7% formaldehyde in PBS and processed for imaging using a 40× objective under a Zeiss LSM 410 inverted confocal laser scanning system. Confocal images were converted to TIFF format and transferred to a Zeiss imaging workstation for pseudocolor presentation.

In Vivo NMHC II-B Phosphorylation in TSU-Pr1 Cells

To measure the in vivo phosphorylation of endogenous NMHC-IIB, 1.2×10^6 TSU-pr1 cells expressing GFP, $PKC\gamma^{WT}$, or $PKC\gamma^{DN}$ were plated on 100-mm dishes ~18 h before the experiment. After 2 h of starvation in RPMI-1640 supplemented with 100 U/ml penicillin, 100 μg/ml streptomycin, and 12 mM HEPES, pH 7.4, cells were stimulated with 7 ng/ml EGF. After stimulation,

cells were lysed in 1.5 ml of 1 x radioimmunoassay precipitation buffer (50 mM Tris pH 7.5, 1% NP-40, 0.5% deoxycholic acid, 50 mM sodium pyrophosphate, 100 mM sodium fluoride and protease inhibitors mix; Sigma). After 10 min incubation on 4°C, lysed cells were scraped from the dishes, transferred to 2 ml tubes and incubated 10 min on ice. Cell debris were pelleted for 15 min by centrifugation at 16,000 × *g*. Each lysate was incubated for 2 h at 4°C on rotary shaker with 120 μl of NMHC-IIB rabbit polyclonal affinity purified antibody prepared in our laboratory. The immunocomplexes were precipitated using 70 μl of protein A-Sepharose (Amersham). After three washes with 500 μl of 1× radioimmunoassay precipitation buffer, 60 μl 2× SDS-PAGE sample buffer were added to the reactions and boiled for 5 min at 100°C. The samples were separated on 7% SDS-PAGE. The amount of NMHC-IIB precipitated was determined by measuring the intensity of NMHC-IIB bands after staining with Coomassie-Blue reagent using the FluorS scanning laser densitometer (Bio-Rad) and FluorS software. The amount of phosphorylated NMHC-IIB was determined by autoradiography using BioMax TranScreen high energy intensifying screen and X-OMAT low sensitivity film (Eastman Kodak, Rochester, NY), and scanning the phosphorylated NMHC-IIB bands with a FluorS scanning laser densitometer and FluorS software. The phosphorylation level of NMHC-IIB was expressed as the ratio of signal intensities obtained from autoradiography and Coomasie staining.

In Vivo GFP-NMHC-IIB Phosphorylation in Transiently Transfected COS-7 Cells

COS-7 cells, 6×10^5, were plated on 60-mm tissue culture dishes 16 h before transfection. Six hours after transfection with NMHC-IIB tagged with GFP constructs, cells were replated on 100-mm tissue culture dishes and incubated 36 h at 37°C in humidified atmosphere. After 4 h starvation in high-glucose DMEM supplemented with 2 mM L-glutamine, 100 U/ml penicillin, 100 μg/ml streptomycin, and 12 mM HEPES, pH 7.4, cells were stimulated with 10 ng/ml EGF and lysed in 1.2 ml of 1× radioimmunoassay precipitation buffer and protease inhibitors mix (Sigma). After 10-min incubation on 4°C, lysed cells were scraped from the dishes, transferred to Eppendorf tubes, and incubated 10 min on ice. Cell debris was pelleted for 15 min by centrifugation at 16,000 × *g*. Each lysate was incubated for 2 h at 4°C on rotary shaker with 24 μl of GFP rabbit polyclonal affinity purified antibody prepared in our laboratory. Immunocomplexes were precipitated using 60 μl of protein A-agarose (Oncogene, Cambridge, MA). After three washes with 500 μl of 1× radioimmunoassay precipitation buffer, 60 μl 2× SDS-PAGE sample buffer was added and boiled for 5 min at 100°C. The samples were separated on 6% SDS-PAGE and stained with SilverSnap Stain Kit II (Pierce, Rockford, IL). The amount of GFP-NMHC-IIB precipitated was determined by measuring the intensity of GFP-NMHC-IIB bands using the ImageMaster VDS-CL imaging system (Amersham) and the densitometry program Fujifilm ImageGauge Ver. 3.4. The amount of phosphorylated GFP-NMHC-IIB was determined by phosphoroimaging using Fujix Bas 2000 bioimage analyzer and Fujifilm ImageGauge Ver. 3.4 software (Tokyo, Japan). The phosphorylation level of GFP-NMHC-IIB was expressed as the ratio of signal intensities obtained from phosphoroimaging and silver staining.

Mass Spectrometry

Five micrograms of 18-kDa NMHC II-B tail (Ben-Ya'acov and Ravid, 2003) was phosphorylated for 8 h using 500 ng recombinant PKCγ as described above, except for the ATP concentration in the mixture, which was 500 μM instead of 100 μM and [γ-^{32}P]ATP was not present. For the nonphosphorylated reference we used the same amount of NMHC II-B tail that was incubated for 8 h in the same conditions except for the addition of PKCγ. The samples were separated on 12% SDS-PAGE and stained with Coomassie brilliant blue. The phosphorylated and unphosphorylated NMHC II-B tail bands were excised from the gel, reduced, alkylated and digested in-gel using sequencing-grade trypsin (Promega, Madison, WI) as described (Pandey *et al.*, 2000). The peptide mixture was desalted using ZipTip C_{18} column (Millipore, Billerica, MA) and the peptides were eluted using 80% acetonitrile and 1% formic acid. The eluted peptides were directly injected by spraying capillaries (Protana, Toronto, Canada) into a Q-TOF II mass spectrometer (Micromass, Toronto, Canada) equipped with a nanoelectrospray source. MS and MS/MS spectra were measured using 1200 V capillary voltage and the MS/MS collision energy was 20–45 V.

MHCBrod Purification and Determination of Critical Concentration for Filament Assembly

Escherichia coli strain BL-21 containing the pET21c-MHCBrod wild type or MHCBrod-S6D mutant plasmid were grown to OD_{600} = ~0.6 and then induced with 1 mM IPTG for 2 h. Bacteria pellets were lysed with lysis buffer (50 mM Tris-HCl, pH 7.5, 0.8 M NaCl, 10 mM EDTA, 10 mM EGTA, 1 mM DTT, 1 mg/ml lysozyme, and 0.5 mM phenylmethylsulfonyl fluoride) and sonicated. Sonicates were centrifuged and the proteins were precipitated from the supernatant with 10% polyethylenimine (Burgess, 1991) and centrifuged at 16,000 × *g*, followed by boiling to denature all proteins except for the α-helical coiled-coil MHCBrod. The mixture was then centrifuged at 100,000 × *g* and the MHCBrod and MHCBrod-S6D were precipitated from the supernatant using ammonium sulfate to remove the remnants of polyethylenimine. The ammonium sulfate pellet was solubilized in Buffer G (20 mM Tris-HCl, pH 7.5, 600 mM NaCl, 5 mM EDTA, and 1 mM DTT), dialyzed against Buffer C (10 mM Tris-HCl, pH 7.5, 50 mM NaCl, and 2 mM $MgCl_2$), and centrifuged at 100,000 × *g*, and the precipitated proteins were resuspended in buffer G. To determine the critical concentration, the proteins were diluted to 25, 50, 100, 250, and 500 μg/ml in Buffer G. Eighty micrograms of each protein concentration was dialyzed for 4 h in 150 mM NaCl dialysis buffer (10 mM phosphate buffer, pH 7.5, 2 mM $MgCl_2$, and 150 mM NaCl), centrifuged in a TL-100 ultracentrifuge (Beckman Coulter, Fullerton, CA) at 100,000 × *g*, for 1 h at 4°C, and the supernatant and pellet were separated. Twenty micrograms of the supernatant and the pellet that was solubilized in 80 μl Buffer G were loaded on 10% SDS-PAGE. The gels were stained with Coomassie brilliant blue, scanned, and quantified using Fujifilm image analyzer LAS-1000 plus and the densitometry program Fujifilm ImageGauge Ver. 3.4.

Triton Solubility Assay

Fibroblasts (2.5×10^5, B^-/B^- MEF) were plated on 30-mm plates 16 h before the experiment. Twenty-four hours after transfection with GFP-NMHC-IIB or GFP-NMHC-IIB-S6D constructs, cells were washed twice with 1 ml PBS and serum-starved for 24 h in high-glucose DMEM supplemented with 2 mM L-glutamine, 100 U/ml penicillin, 100 μg/ml streptomycin, and 0.1% fatty-acid free bovine serum albumin (Sigma). After starvation, cells were lysed by the addition of 200 μl of lysis buffer (50 mM Tris, pH 7.4, 50 mM NaCl, 5 mM $MgCl_2$, 1% Triton X-100, and protease inhibitors mix; Sigma) to the plates followed by incubation for 10 min at 4°C. The Triton-soluble fractions were collected from the plates and centrifuged for 5 min at 16,000 × *g* to remove the remnants of the insoluble fraction. One hundred microliters of supernatant was removed to fresh tubes, 25 μl of 5× SDS-PAGE sample buffer was added, and the tubes were boiled for 5 min at 100°C. After addition of 120 μl SDS-PAGE sample buffer to the plates, the insoluble fractions were collected and boiled for 5 min at 100°C. After separation on 6% SDS-PAGE, the proteins were transferred onto nitrocellulose membrane for 4 h using TE 62 transfer unit (Amersham). Western blot analysis was performed as described above using affinity-purified specific polyclonal antibody directed against the C-terminus of human NMHC-IIB (Straussman *et al.*, 2001). The Western blots were developed using EZ-ECL Chemiluminescence Detection kit (Biological Industries) and the intensity of GFP-NMHC-IIB bands were analyzed using FujiFilm LAS-3000 Luminescent Image Analyzer and Fujifilm ImageGauge Ver. 3.4 software. In the final calculations of the percentage of NMHC-IIB in the insoluble fractions, the amount of NMHC-IIB in the Triton-soluble fraction was corrected by a factor of two and the intensity of NMHC-IIB in the Triton-insoluble fraction was divided by the sum of the intensities of NMHC-IIB in Triton-soluble and -insoluble fractions.

RESULTS

Phosphorylation of NMHC-IIB by PKC

We have previously shown that, both in vivo and in vitro, at least one PKC isoform is involved in the EGF-dependent NMHC-IIB phosphorylation in TSU-pr1 cells. TSU-pr1 cells express the PKC isoforms: βII, γ, ι, ζ, and ε (Straussman *et al.*, 2001), of which βII and γ belong to the conventional PKC (cPKCs; Newton, 2001). We found that cPKCs, immunoprecipitated from TSU-pr1 cells stimulated with EGF, using antibody raised against the hinge region of cPKCs, exhibited significant NMHC-IIB kinase activity (unpublished data). To investigate whether these cPKCs can directly phosphorylate NMHC-IIB, we subjected recombinant PKCβII and PKCγ to an NMHC-IIB phosphorylation assay as described in *Materials and Methods*. Figure 3A shows that PKCγ, but not PKCβII, could phosphorylate MHCBrod in vitro. To test whether PKCβII is active we used a common PKC substrate, MBP, as positive control. We found that both PKC isoforms were capable of phosphorylating MBP to different extends indicating that PKCβII is active (Figure 3B). Although PKCβII had about sevenfold lower activity than PKCγ activity, we would expect that if PKCβII was able to phosphorylate MHCBrod, this phosphorylation should have been above background (Figure 3B). These results support the finding that PKCγ and not PKCβII phosphorylates MHCBrod. Because the molecular weight of PKCγ (80 kDa) is close to the molecular weight of MHCBrod (70 kDa) and members of the PKC family undergo autophosphorylation

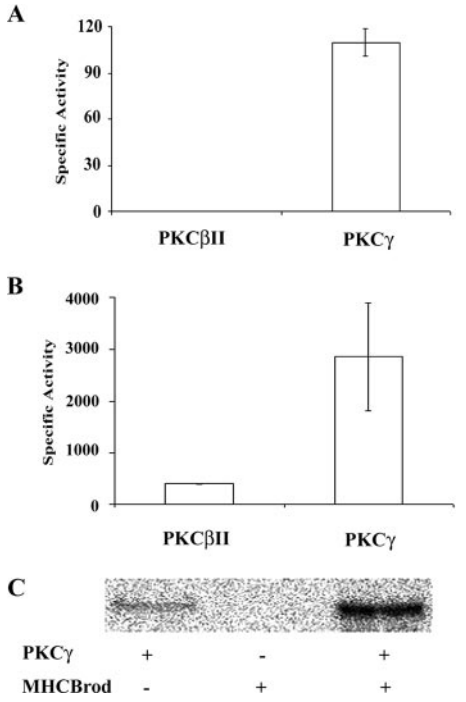

Figure 3. Phosphorylation of NMHC-IIB by recombinant PKCβII and PKCγ. (A) Equal amounts of recombinant human PKCβII and PKCγ were subjected to NMHC-IIB kinase assay as described in *Materials and Methods* with MHCBrod as substrate. The specific activity of each enzyme was expressed as millimoles phosphate incorporated into a mole of MHCBrod per minute per microgram of enzyme. The data shown are the average ± SD of two to three experiments performed in duplicates. (B) Kinase assay with equal amounts of recombinant human PKCβII and PKCγ and common PKC substrate MBP. The specific activity of each enzyme was expressed as millimoles phosphate incorporated into a mole of MBP per minute per microgram of enzyme. The data shown are the average ± SD of two to three experiments performed in duplicate. (C) PKCγ autophosphorylation. Phosphorylation reactions were done as described in *Materials and Methods*. Gels were subjected to phosphoroimaging using Fujix Bas 2000 bioimage analyzer. Lanes 1, reaction was performed with PKCγ only; lane 2, reaction was performed with MHCBrod only; note the complete absence of MHCBrod phosphorylation; lane 3, phosphorylation reaction of MHCBrod by PKCγ. Note the higher amount of phosphate incorporation into MHCBrod compared with lane 1. Shown is a representative experiment with duplicate for each type of reaction.

(Newton, 2001), we wanted to make sure that the phosphorylation detected on MHCBrod is due to phosphorylation by PKCγ (Figure 3A) and not to PKCγ autophosphorylation. For this purpose we subjected PKCγ to autophosphorylation assay, and as shown in Figure 3C, PKCγ indeed undergoes autophosphorylation, but the detected phosphorylation is negligible compared with the phosphorylation of MHCrod by PKCγ. Together, these results indicate that of the two cPKC isoforms expressed in TSU-pr1 cells, PKCγ can directly phosphorylate NMHC-IIB in vitro. It is therefore plausible that PKCγ is the cPKC isoform involved in the EGF-dependent NMHC-IIB phosphorylation.

Identification of PKCγ Phosphorylation Sites on NMHC-IIB

To begin identifying the role of NMHC-IIB phosphorylation by PKCγ, we next mapped the PKCγ phosphorylation sites using mass spectrometry analysis. We used an 18-kDa NMHC II-B C terminal fragment (NMHC-IIB tail; Ben-Ya'acov and Ravid, 2003), phosphorylated by PKCγ to 1.5 mol phosphate per mole substrate as described in *Materials and Methods*. Tryptic peptides were obtained from unphosphorylated and PKCγ-phosphorylated NMHC-IIB tail and dissimilar peaks created by the phosphorylated amino acid residues were subsequently analyzed by MS/MS. The mass spectrometry analysis showed that PKCγ phosphorylates the NMHC-IIB tail at serine residues at positions 1937 (Ser^{1937}) and 1952 (Ser^{1952}) of the full-length of NMHC-IIB and at two additional serine residues lying in a cluster of four serine residues at positions 1935, 1938, 1939, and 1941 of the full-length of NMHC-IIB (Figure 4, A and B). These serine residues are positioned on the nonhelical tailpiece of NMHC-IIB, within a cluster of serine residues that was previously suggested by Murakami *et al.* (1998) as the potential phosphorylation sites for PKC using a mixture of α, β, and γ cPKC isoforms.

To prove that the mapped residues are indeed the phosphorylation sites for PKCγ, we created MHCBrod-S6A construct with serine residues at positions 1937, 1952, 1935, 1938, 1939, and 1941 converted to alanine residues (S6A, Figure 1), as described in *Materials and Methods*, and subjected the resulting protein to a PKCγ phosphorylation assay. As shown in Figure 4C, the conversion of the PKCγ phosphorylation sites to alanine residues caused a marked decrease in MHCBrod-S6A phosphorylation by PKCγ, indicating that the mapped PKCγ phosphorylation sites on MHCBrod are the real sites in vitro.

Because these sites were mapped in vitro, we wanted to verify their relevance for in vivo phosphorylation of NMHC-IIB. For this purpose we used COS-7 cells transiently transfected with NMHC-IIB or NMHC-IIB-S6A, both tagged with GFP, and subjected them to in vivo phosphorylation assay as described in *Materials and Methods*. The COS-7 cell line was chosen because it undergoes EGF-dependent cell motility (Jo *et al.*, 2003) and has high transfection efficiency. As shown in Figure 4D, the ability of NMHC-IIB-S6A to undergo phosphorylation after EGF stimulation was markedly reduced resulting in ~45% decrease in phosphorylation compared with ~30% increase in NMHC-IIB phosphorylation. Thus it seems that the mapped PKCγ phosphorylation sites are relevant for NMHC-IIB phosphorylation in vivo. In addition, we presented evidence that the EGF-dependent NMHC-IIB phosphorylation that occurs in TSU-pr1 was also observed in COS-7 cells, which may indicate that this is a general phenomenon. It should be noted that the peak of NMHC-IIB phosphorylation in TSU-pr1 is 6 min after EGF stimulation (Straussman *et al.*, 2001), whereas in Cos-7 cells the peak is at 2 min. Thus the EGF-dependent NMHC-IIB phosphorylation occurs in different cells with different kinetics.

NMHC-IIB Colocalize with PKCγ in Response to EGF Stimulation

The results presented above indicate that PKCγ is involved in EGF-dependent NMHC-IIB phosphorylation, we therefore, investigated the dynamics of PKCγ and acto-NMHC-IIB cytoskeleton in TSU-pr1 cells stimulated with EGF. Cell motility signals like EGF initiate the formation of lamellipodial extension through massive actin polymerization at the cell's leading edge (Boonstra *et al.*, 1995; Condeelis *et al.*, 2001). To determine whether a similar phenomenon exists in TSU-pr1 cells, we first followed the localization of acto-NMHC-IIB cytoskeleton in response to EGF stimulation using immunofluorescence staining with antibodies specific to the amino-terminus of NMHC-IIB (Ben-Ya'acov and Ravid,

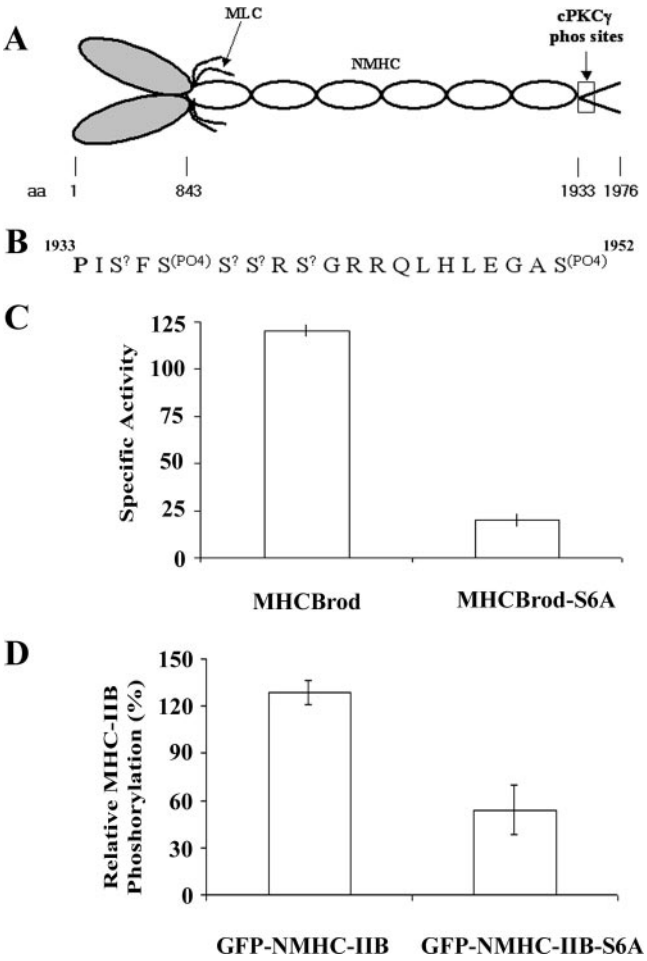

Figure 4. Mapping of PKCγ phosphorylation sites and phosphorylation of NMHC II-B mutants where PKCγ phosphorylation sites were converted to alanine residues. (A) Schematic representation of a myosin II-B molecule; the boxed area represents the region on the nonhelical tailpiece to which the PKCγ phosphorylation sites were mapped. (B) Location of PKCγ phosphorylation sites on NMHC-IIB molecule. Question marks refer to the four serine residues (S^{1935}, S^{1938}, S^{1939}, S^{1941}) of which two of them undergo phosphorylation by PKCγ. P (bold) represents the proline that breaks the α-helical coiled-coil of the molecule. (C) PKCγ kinase activity after converting the mapped phosphorylation sites to alanine residues. MHCBrod and MHCBrod-S6A proteins were subjected to phosphorylation assay with PKCγ, as described in *Materials and Methods*. The specific activity was expressed as millimoles phosphate incorporated into a mole of substrate per minute per microgram of enzyme. The data shown are an average ± SD of two to three experiments performed in duplicates. (D) In vivo phosphorylation of GFP-NMHC-IIB-WT and GFP-NMHC-IIB-S6A immunoprecipitated from COS-7 cells using GFP antibody after 2 min of stimulation with 10 ng/ml EGF. COS-7 cells were transiently transfected with GFP-NMHC-IIB or GFP-NMHC-IIB-S6A constructs and subjected to in vivo phosphorylation assay as described in *Materials and Methods*. The phosphorylation level is expressed as percent of the phosphorylation in unstimulated cells transfected with the same construct. The data are average ±SD of two to three experiments performed in duplicates.

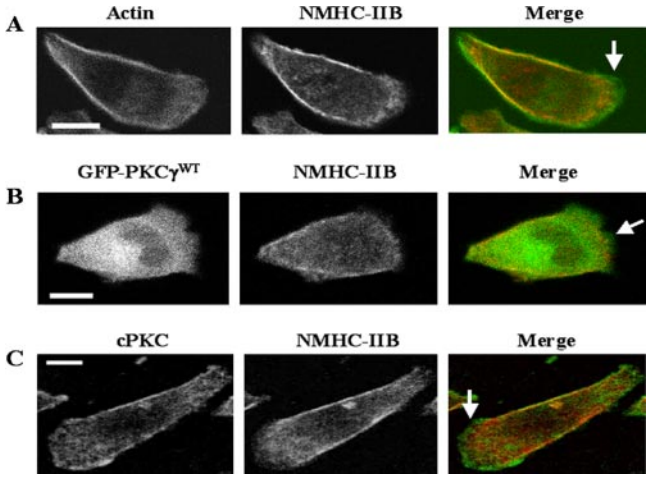

Figure 5. Dynamics of acto-NMHC-IIB cytoskeleton and PKCγ in response to EGF stimulation. TSU-pr1 cells were stimulated with 7 ng/ml EGF for 2 min and subjected to immunofluorescence assays, as described in *Materials and Methods*. (A) Double staining with antibody against the N-terminus of NMHC-IIB and rhodamine-phalloidin. (B) TSU-pr1 cells transiently expressing GFP-PKCγ were stimulated with 7 ng/ml EGF for 2 min and subjected to indirect immunofluorescence using antibody against N-terminus of NMHC-IIB, as described in *Materials and Methods*. (C) Double staining with antibody against the N-terminus of NMHC-IIB and antibody specific to the hinge region of cPKCs. Shown are representative EGF-stimulated TSU-pr1 cells with extended lamellipodia on the leading edge indicated by white arrows. The region of the lamellipodia has a characteristic accumulation of F-actin accompanied by strong staining of cPKCs. This region is poor in NMHC-IIB, which appears only in the transition zone between the lamellipodia and the cell body. Bar, 10 μm.

2003) and rhodamine-phalloidin that recognizes specifically filamentous actin. Lamellipodial extensions observed after EGF stimulation were indeed accompanied by local disruption of cortical acto-NMHC-IIB marginlike structures reflected by extensive acto-NMHC-IIB colocalization (Figure 5A). NMHC-IIB density increased, whereas actin filament density decreased along the lamellipodia from the tip toward the cell body (Figure 5A). This pattern of actin and NMHC-IIB localization is characteristic for lamellipodia (Verkhovsky and Borisy, 1993; Svitkina *et al.*, 1997).

To characterize the localization pattern of PKCγ in EGF-stimulated cells having lamellipodial extensions, we used cells transiently transfected with GFP-PKCγ. First we verified that the fusion protein GFP-PKCγ has activity properties characteristic of cPKC isoforms such as dependence on cofactors. For this purpose we transiently expressed GFP-PKCγ in HEK-293 cells, immunoprecipitated the GFP-PKCγ using GFP antibodies, and subjected it to kinase assay as described in *Materials and Methods*. We found that addition of cofactors was essential for GFP-PKCγ activity, indicating that the fusion of GFP to PKCγ did not affect its activity (unpublished data), these results are consistent with previous reports (Sakai *et al.*, 1997). As shown in Figure 5B, GFP-PKCγ colocalized with NMHC-IIB at the cell cortex close to plasma membrane. In contrast GFP-PKCγ localized to the lamellipodia at the cell's leading edge, whereas NMHC-IIB was absent from this region. To verify that this pattern of GFP-PKCγ localization was not the result of overexpression, we used indirect immunofluorescent staining of cells stimulated with EGF with antibody against the hinge region of cPKCs and antibody against NMHC-IIB (Figure 5C). In these cells, there is a marked enrichment of cPKCs in the lamellipodia at the cell's leading edge, as well as in the posterior region of the cell compared with the cytosolic region. It is therefore possible that the relatively high amount of GFP-PKCγ observed in the cytosolic region of cells expressing this kinase can be the result of GFP-PKCγ

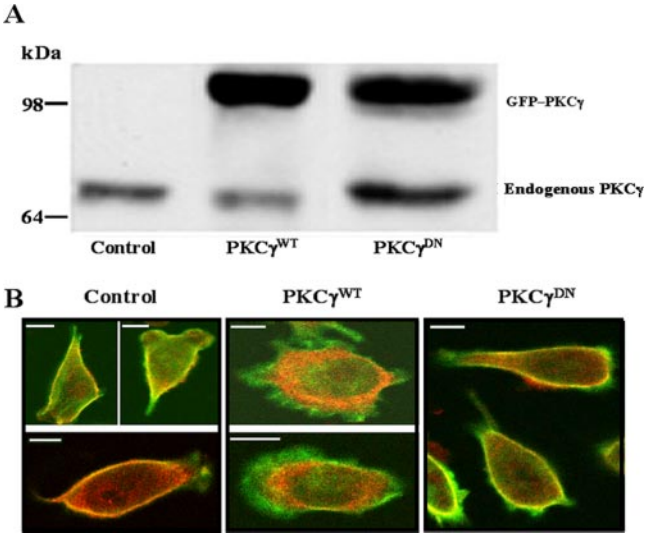

Figure 6. Effect of PKCγ^{WT} and PKCγ^{DN} overexpression on acto-NMHC-IIB cytoskeleton in EGF-stimulated cells. (A) Extracts of TSU-pr1 cell stably expressing PKCγ^{WT} and PKCγ^{DN} were electrophoresed in 10% SDS-PAGE. The proteins were transferred to nitrocellulose membranes and probed with an mAb specific to anti-PKCγ. Cells stably expressing GFP were used as control. kDa, molecular weight marker. (B) TSU-pr1 cells stably expressing PKCγ^{WT} and PKCγ^{DN} fused to GFP were stimulated with EGF for 2 min and subjected to double staining with antibody against N-terminus of NMHC-IIB and rhodamine-phalloidin to visualize actin filaments. Artificial colors were used: green, F-actin and red, NMHC-IIB. Note the strong colocalization of NMHC-IIB and F-actin in the cell cortex of control and PKCγ^{DN} cell lines. This contrasts with cells expressing PKCγ^{WT} in which the acto-NMHC-IIB is disrupted and the cells have wide actin-rich protrusions. GFP channel was omitted for clarity. Representative cells are shown. Bar, 10 μm.

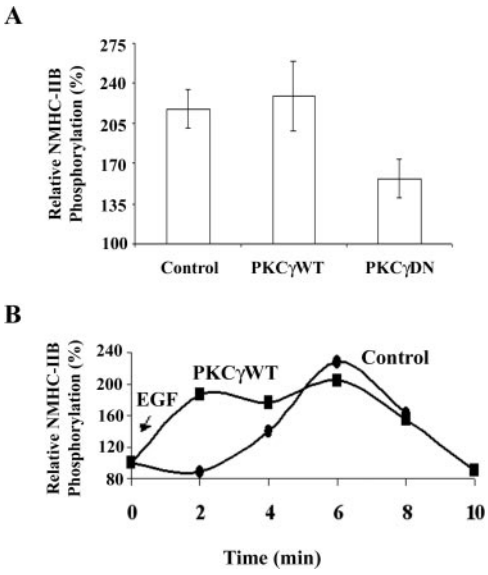

Figure 7. EGF-dependent NMHC-IIB phosphorylation in cells stably expressing PKCγ^{WT} and PKCγ^{DN}. TSU-pr1 cells stably expressing PKCγ^{WT} and PKCγ^{DN} fused to GFP were metabolically labeled with ^{32}P and stimulated with EGF for different time intervals. The phosphorylation level of NMHC-IIB was determined, as described in *Materials and Methods*. (A) NMHC-IIB phosphorylation after 6 min of EGF stimulation in cells stably expressing PKCγ^{WT} and PKCγ^{DN}. The NMHC-IIB phosphorylation is expressed as percent of the NMHC-IIB phosphorylation level 6 min after EGF stimulation compared with unstimulated cells. Data presented are an average ± SD of five and four experiments for PKCγ^{WT} and PKCγ^{DN}, respectively, and three experiments for control cells. (B) A representative kinetics of relative NMHC-IIB phosphorylation in control and cell lines expressing PKCγ^{WT}. Note the faster kinetics of NMHC-IIB phosphorylation in cells expressing PKCγ^{WT} compared with control cells.

overexpression. Colocalization of cPKCs and NMHC-IIB in these cells was also mostly observed in the cell cortex close to the plasma membrane (Figure 5C). Thus, in cells stimulated with EGF, PKCγ has an access to NMHC-IIB and via phosphorylation of NMHC-IIB it may affect the integrity of the acto-NMHC-IIB marginlike structures at the cell's leading edge as well as in posterior regions.

The Effect of PKCγ Overexpression on the Actomyosin Cytoskeleton, Cell Polarity, and NMHC-IIB Phosphorylation after EGF Stimulation

To test the possibility that in TSU-pr1 cells, PKCγ can affect the integrity of acto-NMHC-IIB cytoskeleton, we overexpressed PKCγ wild type (PKCγ^{WT}) and PKCγ dominant negative kinase dead (PKCγ^{DN}) tagged with GFP and studied the effects of the expression of these proteins on NMHC-IIB. The rational for these experiments was that if PKCγ is the isoform responsible for the EGF-dependent NMHC-IIB phosphorylation and cellular localization, then expression of PKCγ^{WT} and PKCγ^{DN} should affect these processes. We created TSU-pr1 cell lines that stably express PKCγ^{WT} and PKCγ^{DN}. The expression level of PKCγ^{WT} and PKCγ^{DN} proteins compared with endogenous PKCγ was estimated as described in *Materials and Methods* and the values obtained were ~10- and ~2-fold for PKCγ^{WT} and PKCγ^{DN}, respectively (Figure 6A).

To examine the effect of PKCγ^{WT} and PKCγ^{DN} expression on the acto-NMHC-IIB cytoskeleton, the stably expressing cell lines were stained for NMHC-IIB and F-actin using specific antibodies for NMHC-IIB and rhodamine-phalloidin, respectively. As shown in Figure 6B, GFP (control) and PKCγ^{WT} cells exhibited broad lamellipodia and disrupted acto-NMHC-IIB marginlike structures, whereas PKCγ^{DN} cell lines presented lamellipodial extensions containing acto-NMHC-IIB boundarylike structures. Thus, overexpression of PKCγ^{WT} affected cell cytoskeleton, possibly by diminishing formation of the acto-NMHC-IIB boundary structure and, thus, allowing high protrusive activity that results in wide lammellipodial extensions (Figure 6B).

However, as PKC isoforms play a role in many biological processes that affect cytoskeleton, such as the regulation of actin polymerization (Keenan and Kelleher, 1998) and myosin light chain phosphorylation (Bresnick, 1999; Iwabu *et al.*, 2004), the effects we described above could be due to the role of PKCγ on these processes. To determine whether the phenotype observed results from a PKCγ effect on NMHC-IIB, we examined the EGF-dependent NMHC-IIB phosphorylation in control, PKCγ^{WT}, and PKCγ^{DN} cell lines. We measured the kinetics of NMHC-IIB phosphorylation after EGF stimulation by immunoprecipitating NMHC-IIB from EGF-stimulated cells that were metabolically labeled with ^{32}P as described in *Materials and Methods*. All three cell lines showed an increase in NMHC-IIB phosphorylation after EGF stimulation, yet the EGF-dependent NMHC-IIB phosphorylation in PKCγ^{DN} cells was 60% lower than that of control cells (Figure 7A). These results indicate that PKCγ is involved in EGF-dependent NMHC-IIB phosphorylation in

vivo. The incomplete inhibition of EGF-dependent NMHC-IIB phosphorylation in PKCγ^{DN} cells may indicate that PKCγ is not the only kinase that phosphorylates NMHC-IIB, other kinases like CKII and members of the PKC family other than PKCγ (Murakami *et al.*, 1984, 1998; Straussman *et al.*, 2001) may also phosphorylate NMHC-IIB. Another possibility is that the expressed PKCγ^{DN} did not inhibit completely the activity of the endogenous PKCγ.

Overexpression of PKCγ^{WT} reached a maximal level of NMHC-IIB phosphorylation similar to that in control cells (Figure 7A). However, the peak of NMHC-IIB phosphorylation in PKCγ^{WT} cells appeared earlier than in control cells and remained up to 6 min after EGF stimulation, before declining (Figure 7B). This difference may be due to high amount of activated PKCγ^{WT} after EGF stimulation resulting in faster kinetics of NMHC-IIB phosphorylation with consequent disruption of acto-NMHC-IIB cytoskeleton.

The Effect of the Replacement of PKCγ Sites by Aspartate Residues on NMHC-IIB Localization

Murakami *et al.* (1998, 2000) have shown that the critical concentration for NMHC-IIB fragment assembly being significantly higher for NMHC-IIB fragment with four PKC sites converted to aspartate residues than that of the wild-type NMHC-IIB fragment. To explore the possibility that the critical concentration for MHCBrod assembly is affected by PKCγ phosphorylation, we created a MHCBrod in which all six PKCγ phosphorylation sites were mutated to aspartate residues (S6D, Figure 1). The MHCBrod-S6D protein also exhibited marked increase in the critical concentration for assembly compared with control wild-type MHCBrod: 100 and 15 μg/ml, respectively.

To examine the in vivo effects of NMHC-IIB phosphorylation by PKCγ on its cellular localization, we created full-length NMHC-IIB fused to GFP in which the PKCγ phosphorylation sites were converted to aspartate residues (NMHC-IIB-S6D). We predicted that, if formation of acto-NMHC-IIB marginlike structures requires NMHC-IIB filament assembly and that phosphorylation of NMHC-IIB by PKCγ leads to local disassembly of these structures, then NMHC-IIB-S6D will exhibit lower assembly at the cell cortex compared with wild-type NMHC-IIB. To test this hypothesis, we transiently transfected TSU-pr1 cells with wild-type NMHC-IIB-WT or NMHC-IIB-S6D fused to GFP, stimulated the cells with EGF and monitored their localization as described in *Materials and Methods.* The level of NMHC-IIB expression in TSU-pr1 was ~1% of the endogenous NMHC-IIB (unpublished data). It is possible that exogenous expression of NMHC-IIB in cells that express NMHC-IIB have some toxic effect, leading to a low expression of the exogenous protein (Landsverk and Epstein, 2005). Although both NMHC-IIB-WT and NMHC-IIB-S6D were able to localize at the cell cortex, the amount of NMHC-IIB-S6D in the cell cortex seemed to be lower than that of NMHC-IIB-WT (Figure 8A). To verify that localization of NMHC-IIB-WT to the cell cortex requires filament assembly, we expressed, in TSU-pr1 cells, NMHC-IIB with a deletion of 278 amino acids from the C-terminal region. This region contains the domains critical for filament assembly of NMHC-IIB (Nakasawa *et al.*, 2005). Figure 8A shows that this deletion abolished the cell cortical localization of this mutated NMHC-IIB. This result supports the idea that filament assembly is required for localization of NMHC-IIB to the cell cortex in EGF-stimulated TSU-pr1 cells.

To quantify the amount of the expressed NMHC-IIB at the cell cortex, we developed a cortical index parameter that is the fraction of the cell cortex occupied by expressed NMHC-IIB, as described in *Materials and Methods*. This index range from zero to one, where zero indicate the absence of NMHC-IIB in the cell cortex and one indicates that the entire cell cortex area is occupied by expressed NMHC-IIB. As shown in Figure 8B, 72 and 46% of cells expressing NMHC-IIB-S6D and NMHC-IIB-WT, respectively, had a low cortical index (0–0.5). Furthermore, only 28% of NMHC-IIB-S6D cells had

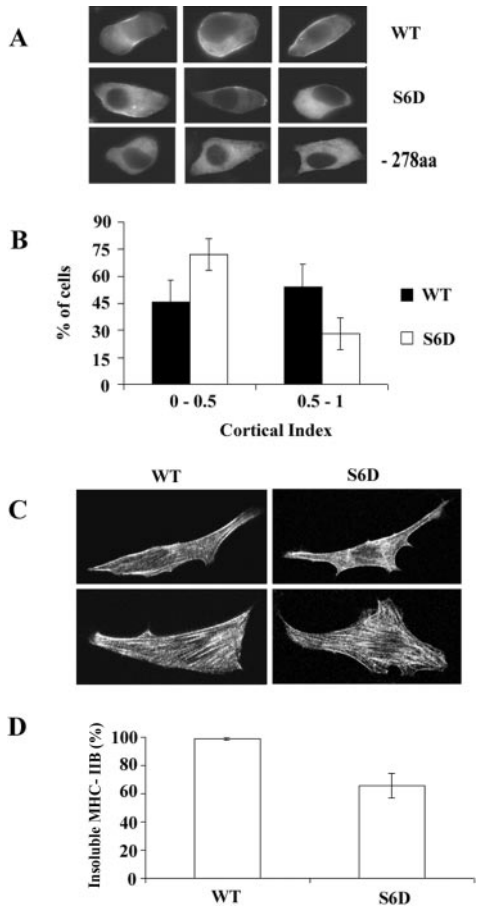

Figure 8. NMHC-IIB-S6D localization to cytoskeleton. (A and B) TSU-pr1 cells were transiently transfected with NMHC-IIB or NMHC-IIB-S6D fused to GFP as described in *Materials and Methods* and stimulated with EGF for 2 min. (A) Representative cells showing localization of NMHC-IIB, NMHC-IIBS6D, and NMHC-IIB with 278 amino acid deletion tagged with GFP. (B) Cortical index measurement of NMHC-IIB and NMHC-IIB-S6D proteins localized to the cell cortex of EGF-stimulated cells. Cells (n = 35–55) were randomly selected for each expressed protein. Cortical index parameter was determined for each cell, as described in *Materials and Methods*. Cells were divided arbitrarily into two subgroups according to the cortical index parameter (i.e., 0–0.5 and 0.5–1) and the percent of cells in each subgroup was estimated relative to total number of cells in the sample. The results shown are the average of three experiments ± SD. (C and D) Mouse embryonic fibroblasts ablated for NMHC-IIB were transiently transfected with NMHC-IIB or NMHC-IIB-S6D tagged with GFP as described in *Materials and Methods*. (C) Representative cells showing localization of NMHC-IIB-WT and NMHC-IIB-S6D. Note the localization of both proteins to stress fibers and cortical region. (D) Triton X-100 solubility of NMHC-IIB-WT and NMHC-IIB-S6D in serum-starved cells. Cells were subjected to Triton X-100 solubility assay, and the percent of total NMHC-IIB and NMHC-IIB-S6D in the insoluble fraction (cytoskeleton) was determined, as described in *Materials and Methods*. Data presented are the average ± SD of four independent experiments.

high cortical index (0.5–1) compared with 54% of NMHC-IIB-WT. These results indicate that expression of NMHC-IIB-S6D causes certain instability of acto-NMHC-IIB margin-like structures, resulting in a reduced population of cells with high cortical index.

Because TSU-Pr1 cells express NMHC-IIB, the intracellular behavior of NMHC-IIB-S6D expressed in these cells can be affected by interaction with the endogenous NMHC-IIB, which can mask the real effect of NMHC-IIB phosphorylation. In addition, as mentioned above, the level of NMHC-IIB expression in TSU-pr1 was ~1% of the endogenous NMHC-IIB. Therefore, we transiently expressed NMHC-IIB and NMHC-IIB-S6D in a cell line of mouse embryonic fibroblasts ablated for NMHC-IIB (Tullio *et al.*, 1997) and subjected these cells to prolonged serum starvation, which was previously shown to induce assembly of stress fibers (Giuliano and Taylor, 1990), which are structures containing bipolar myosin II filaments (Langanger *et al.*, 1986; Svitkina *et al.*, 1989). As shown in Figure 8C, it seems that NMHC-IIB-WT and NMHC-IIB-S6D have similar localization to the cell cortex and to stress fibers. Because immunofluorescence technique is not quantitative, we determined the amount of expressed NMHC-IIB and NMHC-IIB-S6D that localizes with the cytoskeleton using a Triton X-100 solubility assay as described in *Materials and Methods*. As shown in Figure 8D, the percent of insoluble NMHC-IIB-S6D was significantly lower than that of NMHC-IIB. Thus it seems that phosphorylation of NMHC-IIB by PKCγ inhibits its assembly presumably by increasing the critical concentration required for filament assembly. The difference in the behavior of expressed NMHC-IIB-S6D in cells having endogenous NMHC-IIB (TSU-pr1) versus cells that do not express this myosin II (fibroblasts B^-/B^-) may indicate that in order to examine the behavior of myosin II isoforms, one should use cell lines that are ablated for this particular isoform.

DISCUSSION

The acto-myosin II cytoskeleton plays an importance in cell motility (Lauffenburger and Horwitz, 1996; Mitchison and Cramer, 1996). This was first demonstrated in the amoeba *D. discoideum*; the polarity of cell movement was severely impaired in myosin II knockout cells, although general motility remained intact (Spudich, 1989). Along with its participation in rear retraction, myosin II was thought to suppress lateral protrusive activities, allowing the cell to extend an actin-rich pseudopod exclusively from its leading edge, this establishes the polarity of movement.

In the present study we provide evidence for the involvement of PKCγ in the regulation of myosin IIB via heavy chain phosphorylation. We showed that PKCγ phosphorylates directly a 70-kDa C-terminal fragment and that PKCγ colocalized with NMHC-IIB in the cell cortex. We further observed that protrusions at the cell's leading edge were enriched with actin and PKCγ, whereas NNMHC-IIB was absent from these regions. A similar pattern was observed using an antibody against cPKC isoforms. In addition, overexpression of $PKC\gamma^{WT}$ and $PKC\gamma^{DN}$ affected the dynamics of NMHC-IIB phosphorylation. Overexpression of $PKC\gamma^{WT}$ resulted in much faster kinetics of NMHC-IIB phosphorylation and disruption of proper organization of acto-NMHC-IIB cytoskeleton. This can be the result of the fast kinetics of PKCγ activation as recent report suggests that the mechanism of PKCγ activation differs from that of other members of cPKC in that that PKCγ can respond to diacylglycerol even without an increase in intracellular calcium (Ananthanarayanan *et al.*, 2003). A premature rise in NMHC-IIB phosphorylation in stimulated $PKC\gamma^{WT}$ cells can lead to premature disruption of acto-NMHC-IIB marginlike structures, leading to the formation of broad lamellipodia and multiple actin-rich protrusions (Figure 6B). In contrast, overexpression of $PKC\gamma^{DN}$ significantly reduced the level of NMHC-IIB phosphorylation, with the acto-NMHC-IIB cytoskeleton remaining intact even at the leading edge. Furthermore, expression of NMHC-IIB in which the PKCγ sites were converted to aspartate residues, thus mimicking the phosphorylation state of NMHC-IIB by PKCγ, caused a reduction in the amount of this mutated NMHC-IIB in the cell cortex in TSU-Pr1 cells and a significant decrease in its localization to cell cytoskeleton in NMHC-IIB knockout fibroblasts. Thus, PKCγ phosphorylation of NMHC-IIB regulates its assembly, presumably by decreasing its ability to form filaments.

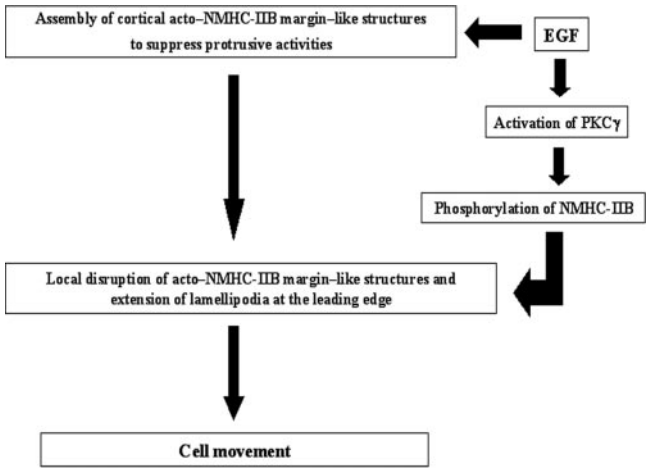

Figure 9. A model for the regulation of NMHC-IIB through its heavy chain phosphorylation during cell migration. See *Discussion* for more details.

Expression of $PKC\gamma^{DN}$ in TSU-pr1 cells did not inhibit the EGF-dependent NMHC-IIB phosphorylation completely (Figure 7A), suggesting that additional kinase(s) might be involved in NMHC-IIB phosphorylation. Resent studies from our laboratory suggest that the p21-activated kinase 1 (PAK1) is also involved in the regulation of NMHC-IIB phosphorylation (Even-Faitelson *et al.*, 2005), and this regulation is mediated by atypical PKCζ (aPKCζ) that directly phosphorylates NMHC-IIB on a single serine residue ~1 min after EGF stimulation (L. Even-Faitelson and S. Ravid, unpublished results). It is therefore plausible that the early phosphorylation of NMHC II-B by aPKCζ after EGF stimulation destabilizes the NMHC-IIB filaments and primes other phosphorylation events carried out by PKCγ.

Taken together, the results presented here allows us to propose a model for the regulation of NMHC-IIB through its heavy chain phosphorylation by PKCγ during cell migration (Figure 9). In unstimulated cells, NMHC-IIB is mostly diffusely distributed within the cytosol (Straussman *et al.*, 2001). EGF stimulation results in translocation of NMHC-IIB to the cell cortex, where it associates with actin filaments to create acto-NMHC-IIB marginlike structures. At the same time there is an asymmetric activation of phospholipase C γ, resulting in a high concentration of cPKC lipid activators at the cell's leading edge (Chou *et al.*, 2003). This results in the preferential translocation of PKCγ to the membrane of the cell's leading edge and subsequent activation. NMHC-IIB in the cell cortex adjacent to the leading edge is exposed to the

activated PKCγ, leading to its phosphorylation and to a local disruption of acto-NMHC-IIB margins at the leading edge. This enables the cell to extend actin-rich lamellipodia. The local disruption of acto-NMHC-IIB can be mediated solely by activated PKCγ or by this together with additional signaling proteins. At the posterior region of the cell, acto-NMHC-IIB margins remain intact providing further support for cell polarity. When a cell translocates, it must retract its posterior part, requiring the disassembly of the acto-NMHC-IIB margins, which is achieved by NMHC-IIB phosphorylation. Our previous findings indicate that acto-NMHC-IIB margin disruption correlates with a peak of NMHC-IIB phosphorylation, increased Triton solubility and its return to the cytosol (Straussman *et al.*, 2001; Even-Faitelson *et al.*, 2005). NMHC-IIB phosphorylation in this region can also be mediated directly by PKCγ or in concert with other kinase(s). Thus, our model suggests that the link between EGF receptor activation and transient NMHC-IIB phosphorylation is activation of PKCγ, as part of a general mechanism for establishing cell movement.

ACKNOWLEDGMENTS

We thank Dr. Mark Tarshis and Dr. Ofra Moshel for their excellent technical assistance with confocal laser microscopy experiments and mass spectrometry, respectively. We also thank the members of S.R.'s laboratory for insightful comments and support. This work was supported by grants from Israel Academy for Sciences and Humanities, Israel Cancer Research Foundation, Israel Ministry of Health, and Israel Cancer Association.

REFERENCES

Ananthanarayanan, B., Stahelin, R. V., Digman, M. A., and Cho, W. (2003). Activation mechanisms of conventional protein kinase C isoforms are determined by the ligand affinity and conformational flexibility of their C1 domains. J. Biol. Chem. *278*, 46886–46894.

Bao, J., Jana, S. S., and Adelstein, R. S. (2005). Vertebrate nonmuscle myosin II isoforms rescue small interfering RNA-induced defects in COS-7 cell cytokinesis. J. Biol. Chem. *280*, 19594–19599.

Ben-Ya'acov, A., and Ravid, S. (2003). Epidermal growth factor-mediated transient phosphorylation and membrane localization of myosin II-B are required for efficient chemotaxis. J. Biol. Chem. *278*, 40032–40040.

Boonstra, J., Rijken, P., Humbel, B., Cremers, F., Verkleij, A., and van Bergen en Henegouwen, P. (1995). The epidermal growth factor. Cell Biol. Int. *19*, 413–430.

Bresnick, A. R. (1999). Molecular mechanisms of nonmuscle myosin-II regulation. Curr. Opin. Cell Biol. *11*, 26–33.

Burgess, R. R. (1991). Use of polyethyleneimine in purification of DNA-binding proteins. Methods Enzymol. *208*, 3–10.

Chou, J., Burke, N. A., Iwabu, A., Watkins, S. C., and Wells, A. (2003). Directional motility induced by epidermal growth factor requires Cdc42. Exp. Cell Res. *287*, 47–56.

Chung, C. Y., Funamoto, S., and Firtel, R. A. (2001). Signaling pathways controlling cell polarity and chemotaxis. Trends Biochem. Sci *26*, 557–566.

Condeelis, J. S., Wyckoff, J. B., Bailly, M., Pestell, R., Lawrence, D., Backer, J., and Segall, J. E. (2001). Lamellipodia in invasion. Semin. Cancer Biol. *11*, 119–128.

Conti, M. A., Sellers, J. R., Adelstein, R. S., and Elzinga, M. (1991). Identification of the serine residue phosphorylated by protein kinase C in vertebrate nonmuscle myosin heavy chains. Biochemistry *30*, 966–970.

De La Cruz, E. M., and Ostap, E. M. (2004). Relating biochemistry and function in the myosin superfamily. Curr. Opin. Cell Biol. *16*, 61–67.

de la Roche, M. A., and Cote, G. P. (2001). Regulation of *Dictyostelium* myosin I and II. Biochim. Biophys. Acta *1525*, 245–261.

Dulyaninova, N. G., Malashkevich, V. N., Almo, S. C., and Bresnick, A. R. (2005). Regulation of myosin-IIA assembly and Mts1 binding by heavy chain phosphorylation. Biochemistry *44*, 6867–6876.

Even-Faitelson, L., Rosenberg, M., and Ravid, S. (2005). PAK1 regulates myosin II-B phosphorylation, filament assembly, localization and cell chemotaxis. Cell Signal. *17*, 1137–1148.

Giuliano, K. A., and Taylor, D. L. (1990). Formation, transport, contraction, and disassembly of stress fibers in fibroblasts. Cell Motil. Cytoskelet. *16*, 14–21.

Golomb, E., Ma, X., Jana, S. S., Preston, Y. A., Kawamoto, S., Shoham, N. G., Goldin, E., Conti, M. A., Sellers, J. R., and Adelstein, R. S. (2004). Identification and characterization of nonmuscle myosin II-C, a new member of the myosin II family. J. Biol. Chem. *279*, 2800–2808.

Iizumi, T., Yazaki, T., Kanoh, S., Kondo, I., and Koiso, K. (1987). Establishment of a new prostatic carcinoma cell line (TSU-pr1). J. Urol. *137*, 1304–1306.

Iwabu, A., Smith, K., Allen, F. D., Lauffenburger, D. A., and Wells, A. (2004). Epidermal growth factor induces fibroblast contractility and motility via a protein kinase C delta-dependent pathway. J. Biol. Chem. *279*, 14551–14560.

Jo, M., Thomas, K. S., O'Donnell, D. M., and Gonias, S. L. (2003). Epidermal growth factor receptor-dependent and -independent cell-signaling pathways originating from the urokinase receptor. J. Biol. Chem. *278*, 1642–1646.

Katsuragawa, Y., Yanagisawa, M., Inoue, A., and Masaki, T. (1989). Two distinct nonmuscle myosin heavy chain mRNAs are differently expressed in various chicken tissues. Eur. J. Biochem. *184*, 611–616.

Kawamoto, S., and Adelstein, R. S. (1991). Chicken nonmuscle myosin heavy chains: differential expression of two mRNAs and evidence for two different polypeptides. J. Cell Biol. *112*, 915–924.

Kawamoto, S., Begur, A. R., Sellers, J. R., and Adelstein, R. S. (1989). In situ phosphorylation of human platelet myosin heavy and light chains by protein kinase C. J. Biol. Chem. *264*, 2258–2265.

Keenan, C., and Kelleher, D. (1998). Protein kinase C and the cytoskeleton. Cell Signal. *10*, 225–232.

Kelley, C. A., Kawamoto, S., Conti, M. A., and Adelstein, R. S. (1991). Phosphorylation of vertebrate smooth muscle and nonmuscle myosin heavy chains in vitro and in intact cells. J. Cell Sci. *14*, 49–54.

Kelley, C. A., Sellers, J. R., Gard, D. L., Bui, D., Adelstein, R. S., and Baines, I. C. (1996). *Xenopus* nonmuscle myosin heavy chain isoforms have different subcellular localizations and enzymatic activities. J. Cell Biol. *134*, 675–687.

Kim, K. Y., Kovacs, M., Kawamoto, S., Sellers, J. R., and Adelstein, R. S. (2005). Disease-associated mutations and alternative splicing alter the enzymatic and motile activity of nonmuscle myosins II-B and II-C. J. Biol. Chem. *280*, 22769–22775.

Kolega, J. (1998). Cytoplasmic dynamics of myosin IIA and IIB: spatial 'sorting' of isoforms in locomoting cells. J. Cell Sci. *111*, 2085–2095.

Kolega, J. (2003). Asymmetric distribution of myosin IIB in migrating endothelial cells is regulated by a rho-dependent kinase and contributes to tail retraction. Mol. Biol. Cell *14*, 4745–4757.

Kovacs, M., Wang, F., Hu, A., Zhang, Y., and Sellers, J. R. (2003). Functional divergence of human cytoplasmic myosin II: kinetic characterization of the non-muscle IIA isoform. J. Biol. Chem. *278*, 38132–38140.

Kuczmarski, E. R., and Spudich, J. A. (1980). Regulation of myosin self-assembly: phosphorylation of *Dictyostelium* heavy chain inhibits formation of thick filaments. Proc. Natl. Acad. Sci. USA *77*, 7292–7296.

Laemmli, U. (1970). Cleavage of structural proteins during the assembly of the head of bacteriophage T4. Nature *227*, 680–685.

Landsverk, M. L., and Epstein, H. F. (2005). Genetic analysis of myosin II assembly and organization in model organisms. Cell Mol. Life Sci. *62*, 2270–2282.

Langanger, G., Moeremans, M., Daneels, G., Sobieszek, A., Debrabander, M., and Demey, J. (1986). The molecular-organization of myosin in stress fibers of cultured-cells. J. Cell Biol. *102*, 200–209.

Lauffenburger, D. A., and Horwitz, A. F. (1996). Cell migration: a physically integrated molecular process. Cell *84*, 359–369.

Li, Z. H., Spektor, A., Varlamova, O., and Bresnick, A. R. (2003). Mts1 regulates the assembly of nonmuscle myosin-IIA. Biochemistry *42*, 14258–14266.

Liang, W., Warrick, H. M., and Spudich, J. A. (1999). A structural model for phosphorylation control of *Dictyostelium* myosin II thick filament assembly. J. Cell Biol. *147*, 1039–1048.

Ludowyke, R. I., Peleg, I., Beaven, M. A., and Adelstein, R. S. (1989). Antigen-induced secretion of histamine and the phosphorylation of myosin by protein kinase C in rat basophilic leukemia cells. J. Biol. Chem. *264*, 12492–12501.

Maupin, P., Phillips, C. L., Adelstein, R. S., and Pollard, T. D. (1994). Differential localization of myosin-II isozymes in human cultured cells and blood cells. J. Cell Sci. *107*, 3077–3090.

Mitchison, T. J., and Cramer, L. P. (1996). Actin-based cell motility and cell locomotion. Cell *84*, 371–379.

Moussavi, R. S., Kelley, C. A., and Adelstein, R. S. (1993). Phosphorylation of vertebrate nonmuscle and smooth muscle myosin heavy chains and light chains. Mol. Cell Biochem. *127–128*, 219–227.

Murakami, N., Chauhan, V.P.S., and Elzinga, M. (1998). Two nonmuscle myosin II heavy chain isoforms expressed in rabbit brains: filaments forming properties, the effects of phosphorylation by protein kinase C and casein kinase II, and location of the phosphorylation sites. Biochemistry *37*, 1989–2003.

Murakami, N., Healy-Louie, G., and Elzinga, M. (1990). Amino acid sequence around the serine phosphorylated by casein kinase II in brain myosin heavy chain. J. Biol. Chem. *265*, 1041–1047.

Murakami, N., Kotula, L., and Hwang, Y.-W. (2000). Two distinct mechanisms for regulation of nonmuscle myosin assembly via the heavy chain: phosphorylation for MIIB and Mts 1 binding for MIIA. Biochemistry *39*, 11441–11451.

Murakami, N., Matsumura, S., and Kumon, A. (1984). Purification and identification of myosin heavy chain kinase from bovine brain. J. Biochem. (Tokyo) *95*, 651–660.

Murakami, N., Singh, S. S., Chauhan, V.P.S., and Elzinga, M. (1995). Phospholipid binding, phosphorylation by protein kinase C, and filament assembly of the COOH terminal heavy chain fragments of nonmuscle myosin II isoforms MIIA and MIIB. Biochemistry *34*, 16046–16055.

Nakasawa, T., Takahashi, M., Matsuzawa, F., Aikawa, S., Togashi, Y., Saitoh, T., Yamagishi, A., and Yazawa, M. (2005). Critical regions for assembly of vertebrate nonmuscle myosin II. Biochemistry *44*, 174–183.

Newton, A. C. (2001). Protein kinase C: structural and spatial regulation by phosphorylation, cofactors, and macromolecular interactions. Chem. Rev. *101*, 2353–2364.

Pandey, A., Andersen, J. S., and Mann, M. (2000). Use of mass spectrometry to study signaling pathways. Sci. STKE *2000*, PL1.

Pasternak, C., Flicker, P. F., Ravid, S., and Spudich, J. A. (1989). Intermolecular versus intramolecular interactions of *Dictyostelium* myosin: possible regulation by heavy chain phosphorylation. J. Cell Biol. *109*, 203–210.

Postma, M., Bosgraaf, L., Loovers, H. M., and Van Haastert, P. J. (2004). Chemotaxis: signalling modules join hands at front and tail. EMBO Rep. *5*, 35–40.

Rosenfeld, S. S., Xing, J., Chen, L. Q., and Sweeney, H. L. (2003). Myosin IIb is unconventionally conventional. J. Biol. Chem. *278*, 27449–27455.

Sakai, N., Sasaki, K., Ikegaki, N., Shirai, Y., Ono, Y., and Saito, N. (1997). Direct visualization of the translocation of the gamma-subspecies of protein kinase C in living cells using fusion proteins with green fluorescent protein. J. Cell Biol. *139*, 1465–1476.

Spudich, J. A. (1989). In pursuit of myosin function. Cell Regul. *1*, 1–11.

Straussman, R., Even, L., and Ravid, S. (2001). Myosin II heavy chain isoforms are phosphorylated in an EGF-dependent manner: involvement of protein kinase C. J. Cell Sci. *114*, 3047–3057.

Svitkina, T. M., Surguchova, I. G., Verkhovsky, A. B., Gelfand, V. I., Moeremans, M., and Demey, J. (1989). Direct visualization of bipolar myosin-filaments in stress fibers of cultured fibroblasts. Cell Motil. Cytoskelet. *12*, 150–156.

Svitkina, T. M., Verkhovsky, A. B., McQuade, K. M., and Borisy, G. G. (1997). Analysis of the actin-myosin II system in fish epidermal keratocytes: mechanism of cell body translocation. J. Cell Biol. *139*, 397–415.

Takahashi, M., Kawamoto, S., and Adelstein, R. S. (1992). Evidence for inserted sequences in the head region of nonmuscle myosin specific to the nervous system. J. Biol. Chem. *267*, 17864–17871.

Tan, J. L., Ravid, S., and Spudich, J. A. (1992). Control of nonmuscle myosins by phosphorylation. Annu. Rev. Biochem. *61*, 721–759.

Tullio, A. N., Accili, D., Ferrans, V. J., Yu, Z. X., Takeda, K., Grinberg, A., Westphal, H., Preston, Y. A., and Adelstein, R. S. (1997). Nonmuscle myosin II-B is required for normal development of the mouse heart. Proc Natl. Acad. Sci. USA *94*, 12407–12412.

Verkhovsky, A. B., and Borisy, G. G. (1993). Non-sarcomeric mode of myosin-II organization in the fibroblast lamellum. J. Cell Biol. *123*, 637–652.

Wang, F., Kovacs, M., Hu, A., Limouze, J., Harvey, E. V., and Sellers, J. R. (2003). Kinetic mechanism of non-muscle myosin IIB: functional adaptations for tension generation and maintenance. J. Biol. Chem. *278*, 27439–27448.